Progress In Electromagnetics Research C, Vol. 106, 239–253, 2020

A Design Methodology for the Implementation of Planar Spiral Antennas with an Integrated Corporate Feed

Paul Tcheg and David Pouhè*

Abstract—A methodology for designing planar spiral antennas with a feeding network embedded within a dielectric is presented. To avoid a purely academic work which may not be manufactured with available standard technologies, the approach takes into account manufacturing process requirements by choice of used materials in the simulation. General design rules are provided. They encompass amongst others, selection criteria for dielectric material, aspects to consider when sketching the radiating element design, as well as those for the implementation of the feeding network. A rule of thumb, which may be helpful in the determination of the antenna supporting substrate's height, has been found. The appeal of the method resides in the fact that it eases up the design process and helps to minimize errors, saving time and money. The approach also enables the design of a compact and small-size spiral antenna as antenna-in-package (AiP), and provides the opportunity to assemble the antenna with other RF components/systems on the same layer stack or on the same integration platform.

1. INTRODUCTION

Since their invention in the 1950s [1, 2], spiral antennas have gained ground and received substantial attention from researchers who have carried out studies concerning their radiating properties and feeding network [3–12]. Their natural broadband characteristic requires a feeding network with wideband features to ensure the desired wideband operation; that is, the impedance bandwidth of both components (antenna and feed) must match. RF equipment such as measuring devices being standardized for 50 Ω-technology and spiral antennas having high input impedance depending on the permittivity of the dielectric material on which they are mounted impedance transformers, known as baluns, are generally used. Well designed, they provide good matching and broadband characteristics. However, their drawback resides in their large physical sizes, thus leading to an overall large volume of the whole antenna.

Fortunately, advances in microelectronic permit the design and manufacture of low-cost and miniaturized systems, which can be used to overcome this drawback. This well-established technology catalyzes changes in antenna technology. It gives opportunities to design spiral antennas with a feed embedded within a dielectric substrate as it is already the case for standard patch antennas. To the knowledge of the authors, at the time being, only one published study by Bosui Liu in [13] has been carried out concerning spiral antennas in this regard. Although his work provides good results, it does not shows any methodology to design a spiral antenna with an integrated corporate feed. It was not the objective he was following.

Designing a spiral antenna and an appropriate feeding network aiming at integrating both into one multilayer printed circuit board (PCB) implies facing a wide range of challenges. These challenges are related to design engineering and manufacturing processes since multilayer PCB design is demanding.

Received 13 July 2020, Accepted 3 November 2020, Scheduled 10 November 2020
* Corresponding author: David Pouhè (david.pouhe@reutlingen-university.de).
The authors are with the School of Engineering, Reutlingen University of Applied Sciences, Alteburgstrasse 150, D-72762 Reutlingen, Germany.

Working out related potential problems also takes an extensive amount of time and requires a highly complex manufacturing process. Therefore, it is worthwhile not only to follow a rational approach to save time and reduce cost but also to ensure accurate results at the end, in particular at high frequencies.

This work addresses these issues. It does not intend to compare different feeding techniques. Instead, it provides a methodology which may be used to design compact spiral antennas with radiating elements and feeding network in the same multilayer PCB by considering manufacture requirements. The aim is to give the antenna engineer a development process which may help him design such antennas to achieve reasonably precise results.

Following these introductory words, the topology and general design criteria are presented in Section 2. Here, due attention is given not only to selection criteria for the substrate and to specific aspects for the design of the integrated feed, but also to the topology in designing the radiating element and optimizing the whole system. The validity and proof of the approach are demonstrated in the third section using a case study. The work ends with some concluding remarks.

2. TOPOLOGY AND GENERAL DESIGN RULES

As for patch antennas, radiation characteristics of spiral antennas when being mounted on a dielectric substrate depend amongst others on the used dielectric material. Designing a compact antenna with an integrated feeding network must, therefore, start with the choice of the adequate substrate followed consecutively by the design and optimization of the radiating element and detailed design of the feeding network.

2.1. Criteria for the Selection of the Adequate Substrate

The first step of the design process involves considering the electrical dimension and the properties of the dielectric material under the radiating structure since the antenna dimensions depend amongst others on the permittivity's characteristics such as loss tangent angle $\tan\delta$. Compared to a spiral antenna surrounded by air, mounting a spiral antenna on a printed circuit board (PCB) considerably affects its well-known intrinsic properties such as broadband impedance, polarization, and radiation pattern. However, system requirements can be met upon properly choosing the dielectric material on which the antenna is mounted. To that end, some guiding criteria for the selection of the adequate substrate are identified as follows.

2.1.1. Dielectric Material with Low Permittivity and Low Loss Tangent

Parameters of the dielectric material are of paramount importance in the operation characteristics of antennas. The permittivity influences the gain and bandwidth while the loss tangent increases with increasing frequencies. Dielectric materials with low loss tangent (0.002 or lower, as a guideline) and of low permittivity over a broad bandwidth (generally the frequency band of interest) are therefore suitable to ensure the broadband characteristic of the antenna. In addition, easy handling of the laminate during the fabrication processes may also be a criterion.

2.1.2. Substrate Thickness

Substrate thickness impacts the bandwidth and power handling capability of patch antennas [14]. For the particular case of spiral antennas on a dielectric substrate, radiation characteristics such as the axial ratio and radiation pattern are most affected by the electrical height of the substrate. As the electrical height increases, the axial ratio deteriorates, and a reduction of the overall effective bandwidth of the spiral antenna follows. Besides, the radiation pattern deteriorates; the gain gets low; and side lobes build up gradually regardless of any dielectric material, as demonstrated in an article to come. It is, therefore, desirable to choose thin material thickness for spiral antennas mounted on an ungrounded substrate.

For the particular case of spiral antennas on a grounded substrate, minimization of effects due to the interplay between the antenna and its ground, such as the excitation of tertiary currents on the radiating element, substantial wave reflections occurring between the antenna and the ground plane

as well as at the arms end, requires consideration of the electrical substrate's height at the lowest chosen analysis frequency to find the minimum substrate's height necessary. To that end, it is helpful to calculate the ratio of the substrate's height (h_{sub}) to the effective wavelength at the low operation frequency f_{low}, that is: $h_{sub}/\lambda_{low,eff}$, where $\lambda_{low,eff} = \lambda_{low}/\sqrt{\varepsilon_{r,eff}}$. A rule of thumb is $h_{sub} \geq \frac{\lambda_{low,eff}}{6}$.

2.1.3. Easy Integration in a Multilayer PCB Using the Standard Manufacturing-Technology

The development of an antenna and its feeding network to achieve an integration of both components into a multilayer PCB to build one single unit is ensured by mechanical as well as electrical properties of the used dielectric interposer. Since a unique production of such materials can be expensive, it is advisable to use standardized materials in order to keep production costs within reasonable budget limits.

2.1.4. Availability of Prepreg

For manufacturing purposes, but also to facilitate the combination of single layers into a multilayer PCB, the antenna designer should ensure that suitable prepreg is available prior to the choice of dielectric material. From the electrical point of view, the compatibility of the substrate and the prepreg is essential to ensure wave propagation within the whole board. Therefore, the dielectric constant and the dielectric loss values of the substrate and prepreg should be roughly identical and comply with the spiral antenna's broadband properties.

2.2. Design and Optimization of the Radiating Element

Once the dielectric material has been selected, the antenna designer can dedicate his attention to the radiating element by following the well-known design principles of spiral antennas found in any standard book on Antenna Theory [17], whose theoretical procedure is shortly reproduced below for completeness.

Curves limiting the edges in one arm of an equiangular spiral antenna are calculated as follows [17]:

$$\rho_1 = \rho_0 \cdot e^{a\varphi} \tag{1a}$$

$$\rho_2 = \rho_0 \cdot e^{a(\varphi-\delta)} \tag{1b}$$

for the inner and outer curves of the antenna's arm, respectively. In Eq. (1), the variation range of φ depends particularly on the ratio ρ_{out}/ρ_0. δ describes the angular width; a is the arm growth ratio; and ρ_0 stands for the initial inner radius of the arm for $\varphi = 0$. The other arm of the antenna is described by the same equations rotated by an angle of π radians.

The inner radius determines the upper limit of the operation frequency f_{up} and vice versa. We have [17]

$$f_{up} \approx \frac{C_0}{2\pi\sqrt{\varepsilon_{r_{eff}}}\rho_0} \tag{2}$$

or

$$\rho_0 \approx \frac{C_0}{2\pi\sqrt{\varepsilon_{r_{eff}}}f_{up}} \tag{3}$$

where $\varepsilon_{r_{eff}} = (\varepsilon_r + 1)/2$ and C_0 is the velocity of light. If the inner radius ρ_0 is specified, Eq. (2) is chosen, else if the upper-frequency limit of the operating bandwidth is known, Eq. (3) should be used. The lower frequency of the operation bandwidth f_{low} is its side obtained from Eq. (4)

$$f_{low} \approx \frac{C_0}{2\pi\sqrt{\varepsilon_{r_{eff}}}\rho_{out}} = \frac{C_0}{2\pi\sqrt{\varepsilon_{r_{eff}}}\rho_0 e^{a\Delta\varphi}}, \tag{4}$$

where Dyson's relation

$$\rho_{out} = \rho_0 e^{a\Delta\varphi} \tag{5}$$

between the outer radius ρ_{out} and the inner radius, ρ_0, has been used.

The operation bandwidth is therefore given by

$$B = \frac{f_{up}}{f_{low}} = e^{a\Delta\varphi} \tag{6}$$

In Eqs. (4) to (6), $\Delta\varphi$ expresses the number of turns of the spiral in radians.

With a chosen arm growth a, the number of turns $\Delta\varphi$ is obtained from Eq. (5) as

$$\Delta\varphi = \frac{\ln \dfrac{\rho_{out}}{\rho_0}}{a}. \tag{7}$$

The relation in Eq. (7) gives the theoretical value of the number of turns. However, is it opportune to construct the radiating element based on this value? Or is this value not just a guideline for dimensioning the antenna?

The answer to the first question is yes if the air surrounds the antenna, and it is no for an antenna mounted on a grounded substrate.

For a spiral antenna mounted on a substrate backed by a ground plane, interactions between the radiating element and the reflecting metal plate as represented by the image of the antenna exist. This interplay is a source of oscillations in the impedance curves at low frequencies (Fig. 6), since the effective substrate's height, $h_{sub}/\lambda_{low,eff}$, is electrically small, compared to its value at high operating frequencies. As a result, substantial impedance variations at the low-frequency range occur. A solution to this issue is to reduce the number of turns, which leads to an increase in the substrate's electrical height and, hence, a reduction of the ground plane's effects. It is, therefore, apparent that the calculated value from the relationship in Eq. (7) is only indicative. On account of the above said, the second question is also answered.

The reduction of the number of turns also leads to a decrease of the outer radius, which results, according to Eq. (4), in an increase of the lower frequency towards higher frequencies at which the substrate's thickness is at least a sixth wavelength or higher. The then obtained new frequency is, in point of fact, the lower frequency of operation. It may be named $f_{low,opband}$, while the lower frequency gained from Eq. (4) using the value calculated from Eq. (7) can be termed lower analysis frequency, $f_{low,anl}$.

2.3. The Feeding Network: Its Design and Implementation

Prior to some specific aspects of the general methodology, we would like to emphasize that, in the following, it is assumed that the dielectric in which the feed is embedded is of the same electrical properties as the one below the radiating element. Of course, it is possible to select two different materials, but this may cause some constraints in the design since the impedance of a conductor depends amongst others on the surrounding media. Two vertical interconnect accesses (vias) with different diameters are, therefore, needed for each arm to connect the spiral with the feeding network, as illustrated in Fig. 1. Issues to be faced with respect to manufacturing processes for a proper alignment as well as for the realization of the plugging process rule out this option.

2.3.1. Determination of the Stripline Thickness

When being embedded in multilayer dielectric media bounded by two conducting planes, the feed, the surrounding material, and the top and bottom metal layers build a stripline structure (Fig. 2) in which the principal TEM mode as well as higher order modes propagate. Since higher-order modes may alter the feed's overall performance, the designer shall ensure that only the TEM mode propagates within the stripline up to the highest analysis frequency, especially at the feed's input. The mathematical description of this waveguide and its intrinsic propagation properties can be combined to determine its thickness. The characteristic impedance is described as [18]:

$$Z_0 = \frac{30\pi}{\sqrt{\varepsilon_r}} \frac{1}{\dfrac{W_e}{b} + 0.441} \tag{8}$$

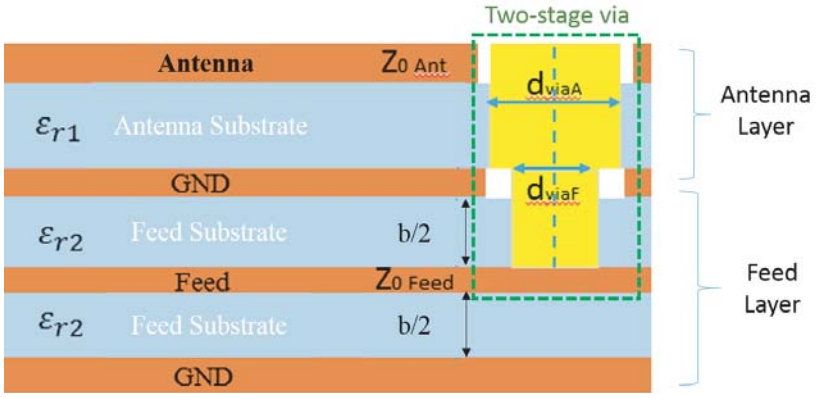

Figure 1. Two-stage via.

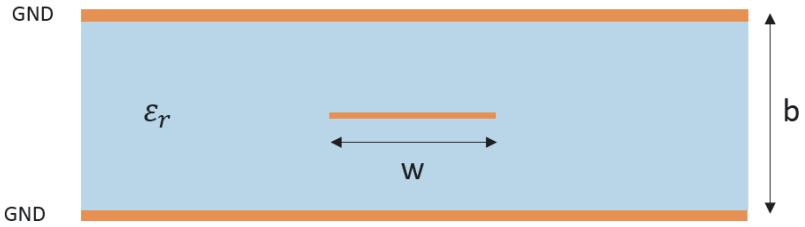

Figure 2. Cross section of the stripline transmission line configuration.

where b and ε_r are the total height of the stripline and the permittivity of the media respectively. W_e is the effective width of the inner conductor given by

$$\frac{W_e}{b} = \frac{W}{b} - \begin{cases} 0, & \frac{W}{b} > 0.35 \\ \left(0.35 - \frac{W}{b}\right)^2, & \frac{W}{b} < 0.35 \end{cases} \tag{9}$$

From Eq. (8), we can get $\frac{W_e}{b}$. Setting this now in Eq. (9) and solving the then obtained equation for $\frac{W}{b}$ yields

$$\frac{W}{b} = \begin{cases} x & \text{for} \quad \sqrt{\varepsilon_r} Z_0 < 120\,\Omega \\ 0.85 - \sqrt{0.6 - x} & \text{for} \quad \sqrt{\varepsilon_r} Z_0 > 120\,\Omega \end{cases} \tag{10}$$

where

$$x = \frac{30\pi}{\sqrt{\varepsilon_r} Z_0} - 0.441 \tag{11}$$

The maximum operating frequency to maintain the TEM properties of stripline at its cross-section (for a given dimension of the inner conductor) is obtained as [19]:

$$f_{\max} = \frac{300}{\sqrt{\varepsilon_r}(2W + \frac{\pi}{2}b)} \quad [\text{GHz}] \tag{12}$$

2.3.2. The Minimum Diameter of the Blind Via, $D_{\min}$

One option to transmit electromagnetic energy from the feeding network towards the antenna is through vias, whereby in the case of the spiral antenna, each arm is connected to a via. In order to avoid impedance mismatch at the interfaces feed-via and via-antenna, it is primordial to determine the diameter of the via. Parameters required for the calculation of the minimum diameter are the overall height of the PCB and the standard aspect ratio of a blind via based on manufacturing requirements.

The overall thickness of the PCB, which includes, to a large part, the thickness of antenna's substrate ($h_{sub,Ant}$) and that of feed's substrate ($h_{sub,Feed}$) determines the needed diameter of vias. The thickness of the prepreg, usually being a quantité negligible compared to the overall thickness of the substrate, was neglected.

2.3.3. Calculation of the Width of the Last Feed's Section and Deduction of the Characteristic Impedance of the Spiral Antenna

The equivalent radius concept may be applied to transform the cylindrical via into a planar inner conductor of the stripline (Fig. 3), whose width (W_{Trace}) is calculated as follows [20]:

$$W_{Trace} = 4r_{via} \tag{13}$$

where r_{via} is the radius of the via, which may also be called electrical equivalent radius.

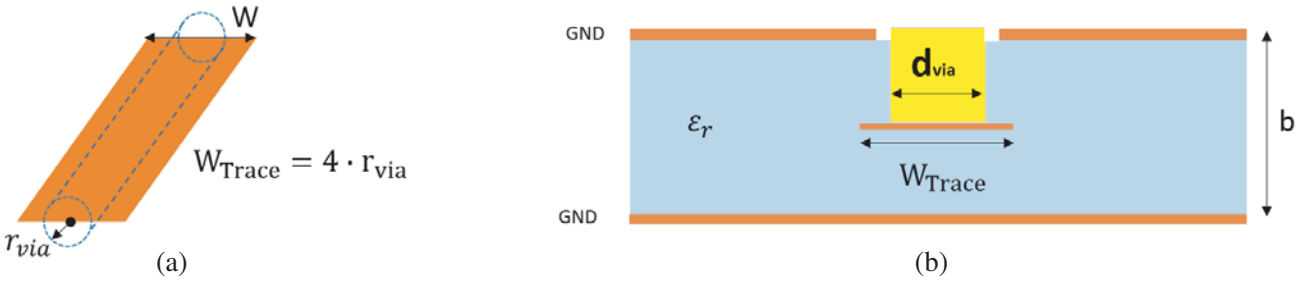

Figure 3. (a) Electrical equivalent radius and (b) illustration of the connection between via and feeding network.

The characteristic impedance of this output section line of the feeding network, and hence of the spiral antenna, is obtained upon applying Eq. (8). The rest of the feeding network can be designed applying the transmission line theory [18] and techniques described in the literature [21, 22].

If the blind via with the obtained diameter corresponding to the characteristic impedance of the radiating element is not producible because of the aspect ratio, an optimization of the spiral antenna taking into consideration manufacturer constraints is called for. The main aspects of the optimization procedure are the reduction of both the number of turns and the inner radius.

2.4. Block Diagram

The approaches developed in the previous sections are summarized in a block diagram (Fig. 4). A detailed description of its differences blocks is not necessary since all steps have already been described above.

3. CASE STUDY AND VALIDATION OF THE PROCEDURE

We would like now to validate the design procedure provided above in light of a case study.

3.1. The Radiating Element

As a starting point, we decided to design an antenna operating in the K- and Ka-bands. We, therefore, set the working frequency at 24 GHz and defined the analysis frequency band between 10 and 40 GHz. In this frequency range, Isola Astra MT77 shows electrical properties that meet the criteria defined in Subsection 2.1.

Following the approach presented in Section 2.2, the radiating element was designed. Eq. (3) whereby $\varepsilon_{r,eff} = 2$ allows us to obtain the inner radius of the spiral as $\rho_0 = 0.84$ mm, whereas from Eq. (5), we get the outer radius ρ_{out} equal to 3.37 mm. Since self-complementary structures provide good antenna characteristics [5], the angular width of the arm δ is set to $\pi/2$.

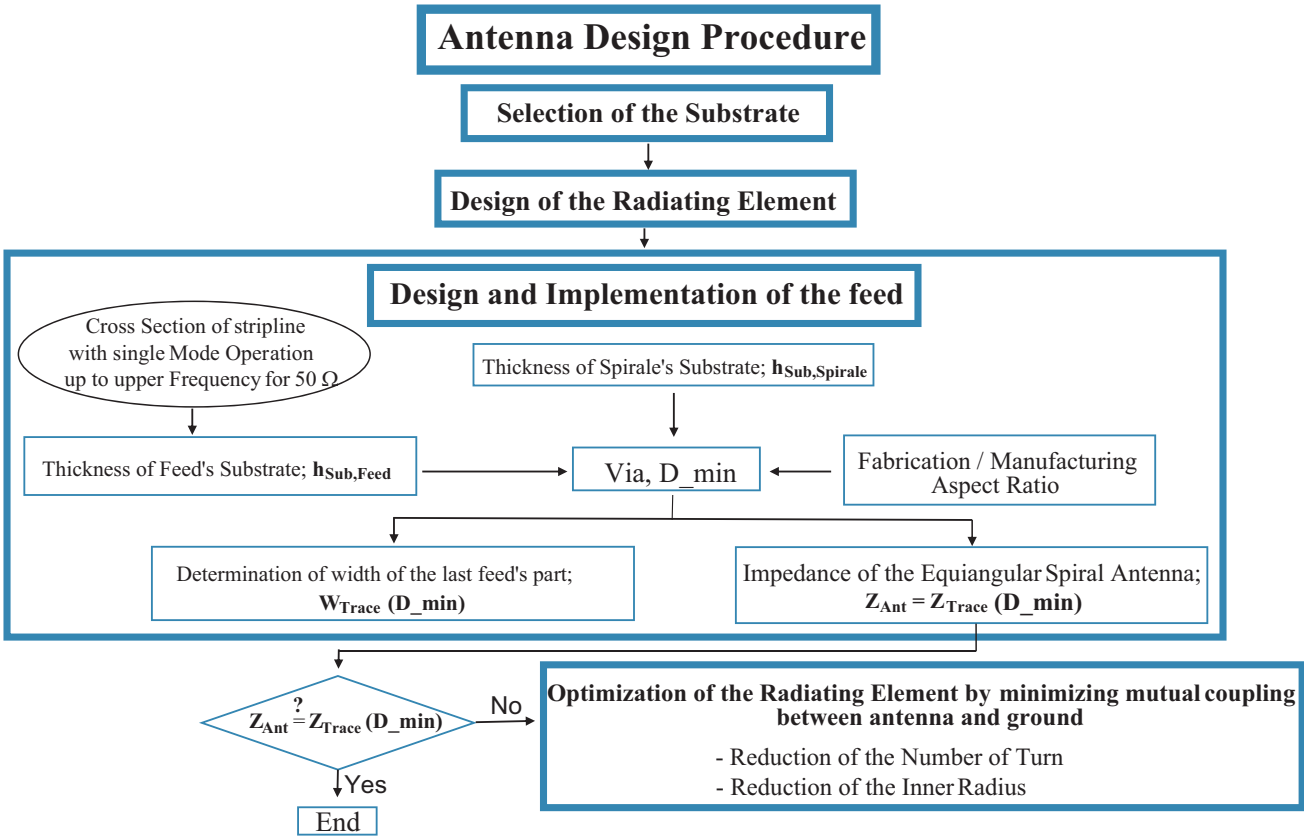

Figure 4. Block diagram summarizing the development process of the spiral antenna with an integrated corporate feed.

Investigations carried out in [24] and [25] show that less tightly wrapped equiangular spiral with an arm expansion between 0.2 and 0.3 can achieve good axial ratio's values. For this reason, the expansion ratio a is chosen to be 0.3 corresponding to an angle $\Psi = \arctan\frac{1}{a} = 73.3°$. a together with ρ_0 and ρ_{out} enable the calculation of the number of turns from Eq. (7) to obtain $\Delta\varphi = 4.63\pi$ radians corresponding approximately to 2.31.

Figure 5 shows the obtained radiating spiral antenna element mounted on a grounded substrate (Astra MT77) to ensure the unidirectional radiation of the electromagnetic field. Based on the Babinet's principle, an impedance $Z = 133\,\Omega$ is obtained and assigned to the lumped port at the center of the structure. Investigation of the impedance variation versus the frequency was carried out with the aim of finding the suitable substrate's height. Ansys HFSS 18.0 is used to that end.

Figure 6 depicts the real part and imaginary part of the impedance chart of the simulated structure. In order to avoid the overload of the figure, only the results of three heights (0.25 mm, 0.75 mm and 1.5 mm) are highlighted, so that the different heights can be better distinguished. The difference of the spectral response of the impedance related to the heights over the frequency can be observed. At low frequencies, where the substrate's height is electrically small, all curves show substantial variations and high resonance peaks. At first glance, this behaviour seems to be only due to the substrate's height. However, the intensities of resonance peaks are less severe when the spiral antenna is mounted on an ungrounded substrate. Thus, the leading cause can be attributed to the ground plane under the dielectric material. Moreover, the conducting plane enhances the effect of the tertiary current in the composed current flowing on spiral arms.

As the height of the substrate increases, the intensity of the resonance peaks starts levelling off with increasing frequencies, and the impedance becomes real and constant for $h_{sub} \geq \lambda_{low,eff}/6$. Therefore, we chose the radiating element of 1.5 mm above the grounding plane for the rest of the work.

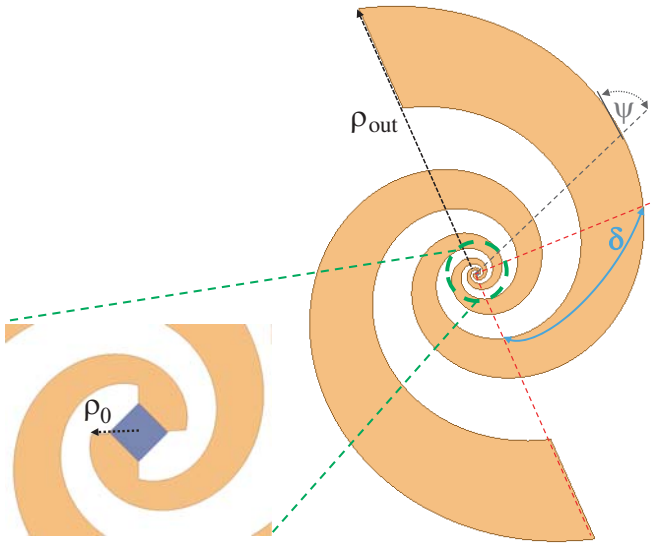

Figure 5. Equiangular spiral antenna for $a = 0.3$, $NT = 2.31$, $\rho_0 = 0.84\,\text{mm}$ and $\rho_{out} = 3.37\,\text{mm}$. The antenna is mounted on the selected substrate, which is backed by a ground plane to ensure the unidirectional radiation of the field.

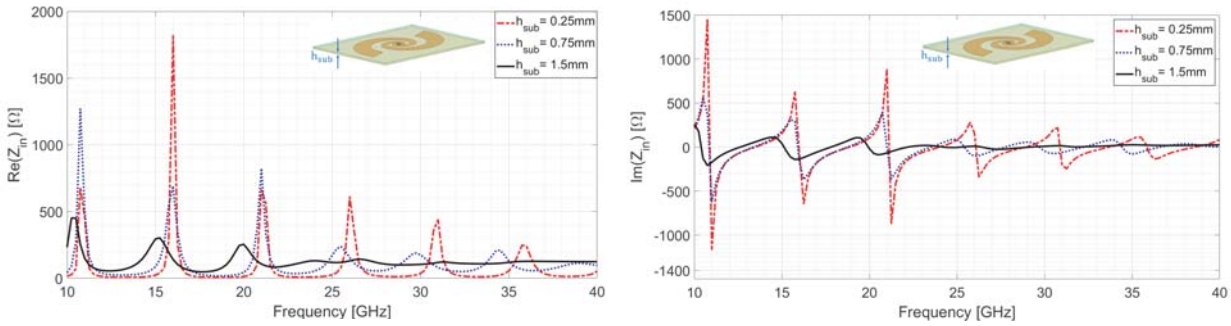

Figure 6. Real and imaginary part of the impedance for different values of the substrate's height.

3.2. The Feeding Network

For the feeding network's design, the characteristic impedance Z_0 is set to $50\,\Omega$. From Eq. (10), we get the ratio W/b equal to 0.6472, which substituted in Eq. (12) for $f_{\max} = 40\,\text{GHz}$ yields $b = 1.511\,\text{mm}$. However, in our simulations, $b = 1.5\,\text{mm}$, this is $0.75\,\text{mm}$ times 2. This value was the maximum substrate's height available at the time we were carrying out the present study [15]. Note that in deriving b we made use of the first equation in Eq. (11).

Following the development in Subsection 2.3.2 and considering the manufacture aspect ratio for blind via of $1:10$ [16], a minimum diameter of 300 μm was found, which, according to Eq. (13), leads to a width $W_{Trace} = 600\,\mu\text{m}$.

Upon setting $W_e = W_{Trace}$ in Eq. (8), the characteristic impedance of the output section line of the feeding network and thus of the spiral antenna is calculated to be $64.7\,\Omega$, which for convenience is approximated to $65\,\Omega$. The rest of the feed is developed according to general accepted microwave techniques for planar corporate feeds [21–23].

Figure 7 presents the designed feeding network. Shorting pins have been added around the input to reduce unwanted modes as well as radiation in the transverse direction to stabilize the line impedance. Their position was determined by analyzing the electromagnetic field in the substrate and applying the frequency sweep approach. The feeding network shows good electrical performance, as can be seen from

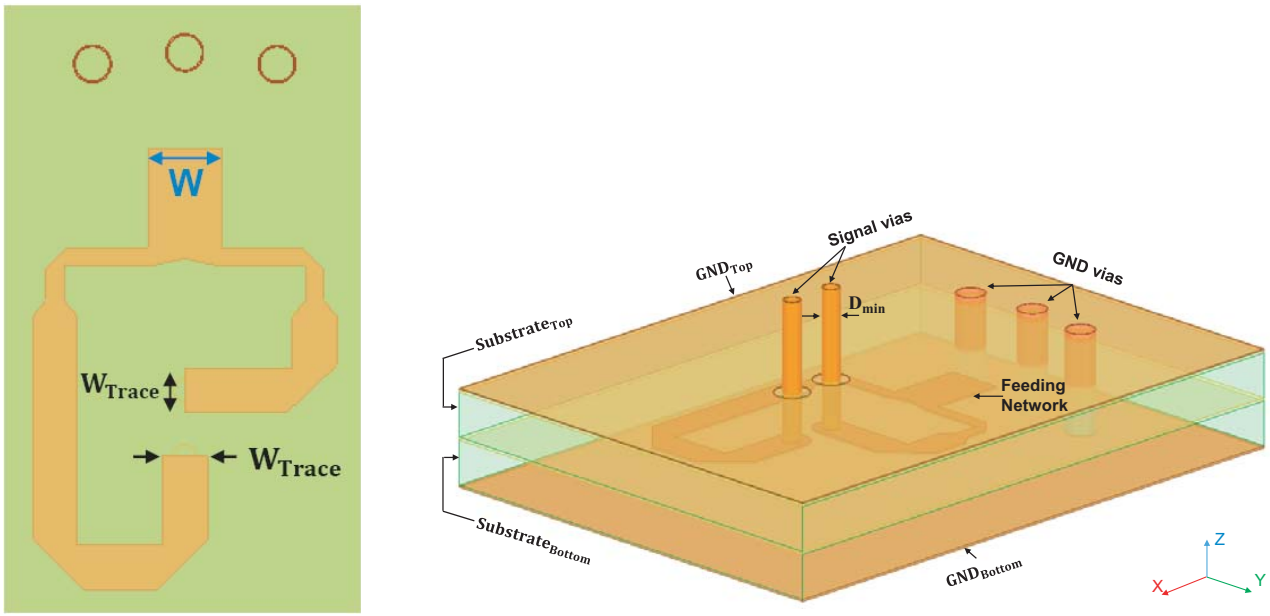

(a) (b)

Figure 7. Designed feeding network. (a) Plan view and (b) 3D-view.

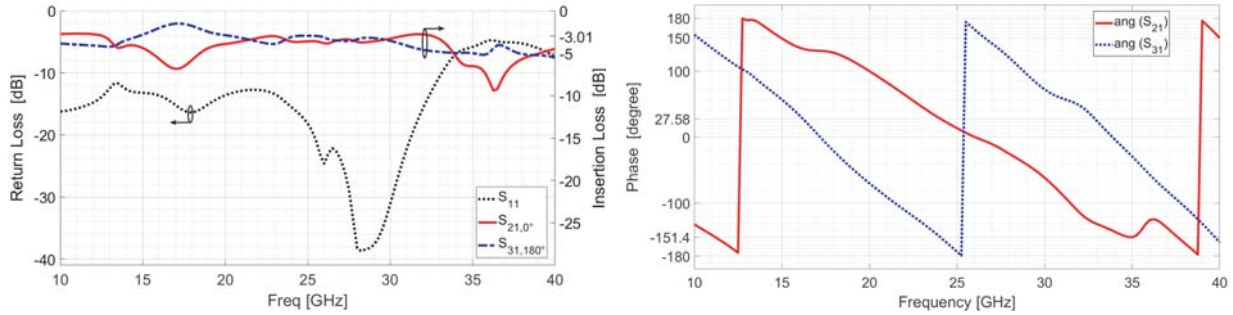

(a) (b)

Figure 8. Electrical characteristics of the feeding network. Input reflection coefficient and (a) insertion loss, (b) phase.

the input reflection coefficient and transmission characteristics (Fig. 8).

Unfortunately, the impedance of 65 Ω differs from that of the radiating element (133 Ω). The later requires a via diameter of 43 µm lower than 300 µm to avoid mismatch between the antenna and its feeding network, a diameter which cannot be produced by the actual standard manufacture technology. An optimization of the radiating element is therefore called for.

3.3. Optimization of the Radiating Element

To ensure impedance matching between the spiral antenna and the corporate feed, the radiating element was optimized by reducing the number of turns along with the reduction of the inner radius. This technique enables decreasing the input impedance from 133 Ω to 65 Ω. The number of turns was decreased from 2.31 to 0.75 leading to an outer radius $\rho_{out} = 2.63$ mm. At the same time, the inner radius was reduced by 0.44 mm to get $\rho_0 = 0.4$ mm. The then obtained radiating element is depicted in Fig. 9 along with its input impedance curve. As can be seen, the antenna has a constant impedance of 65 Ω over a frequency band of about 11.64 GHz, from 20 to 31.64 GHz.

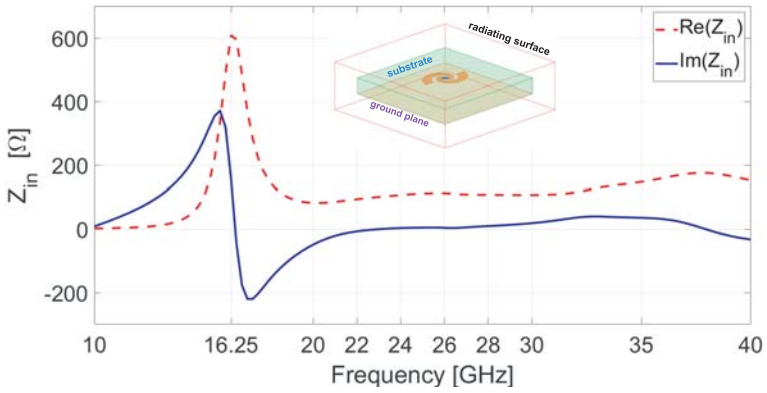

Figure 9. Optimized radiating element (inset) and its input impedance curve.

3.4. The Whole Antenna Structure

The optimized radiating element was combined with the feeding network into an integrated structure, as shown in Fig. 10 and then investigated. Figs. 11 and 12 display some representative results as obtained from simulations.

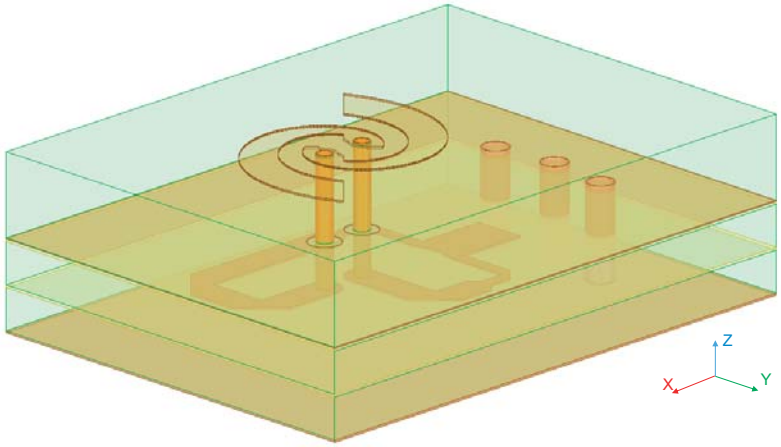

Figure 10. Combined antenna structure fed by a lumped port.

Again, the antenna exhibits good radiation characteristics with an impedance bandwidth of more than 14 GHz, an axial ratio bandwidth of 5.66 GHz at $\vartheta = 0°$ and 11 GHz gain bandwidth with a peak gain of 7.5 dB at 22 GHz. Table 1 summarizes all obtained results.

3.5. Comparison with Experimental Results

The designed whole antenna was manufactured by taking into consideration additional manufacturing requirements, which might influence the performance of the antenna. Parameters belonging to these requirements are amongst others:

- **The prepreg** is used to hold single cores together. Compatibility between electrical properties of the substrate and those of prepreg is essential in ensuring a good wave propagation within the whole board. Dielectric constant and dielectric loss values of both materials must, therefore, be roughly similar.
- **The surface roughness of the PCB** is necessary to hold layers together. However, at high frequencies, it might have adverse influences on the overall performance of the antenna

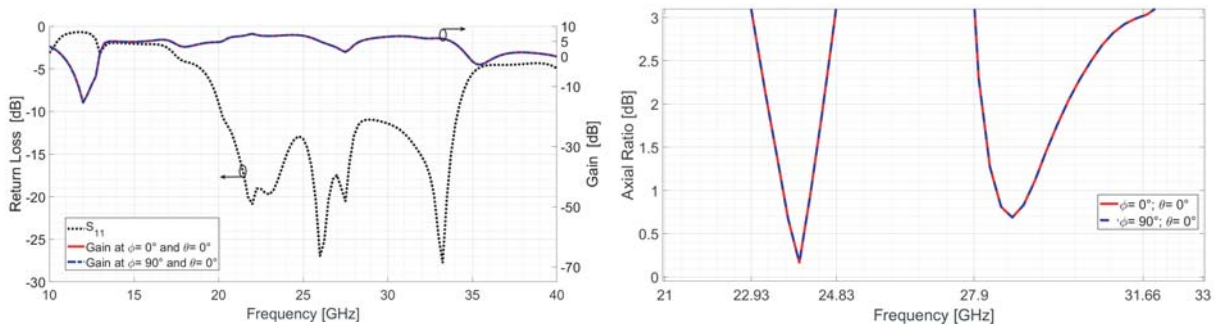

(a) (b)

Figure 11. (a) Reflection factor and gain. (b) Axial ratio of the combined antenna structure fed with a lumped port.

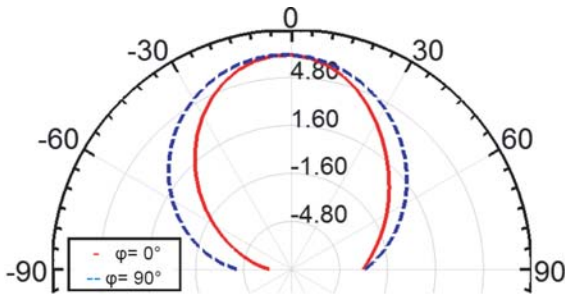

Figure 12. Radiation pattern (simulated) of the combined antenna structure.

Table 1. Summary of obtained results from the simulation of the whole structure.

Parameter	Values
Impedance bandwith	14.06 GHz (20.1–34.16 GHz)
RL @ 24 GHz	−15.02 dB
Max. Gain	7.5 dB @ 22 GHz
Gain (@ $\vartheta = 0°$, and $f = 24$ GHz)	7.05 dB
Axial Ratio bandwidth (@ $\vartheta = 0°$)	5.66 GHz (1.9 GHz + 3.76 GHz)
Bandwidth (Gain >= 5 dB)	11 GHz (5.73 GHz + 5.5 GHz)

since conductor loss increases, leading thus to substantial discrepancies between simulated and experimented data, if not previously taken into account in the simulation.

- **The backdrill process on all GND vias** to avoid any electrical contact between the top layer and GND planes, as well as undesired radiation rising from L3 over the antenna's substrate and L1 to the free space.

The fabricated antenna and its layer stack structure are presented in Fig. 13 while Fig. 14 displays the measurement setup. It consists of a Rhode & Schwarz ZVA network analyzer, an RF cable, and the AUT. Connection with the network analyzer through a cable was ensured through a coaxial K-connector added at the connection point of the corporate feed. The antenna has the following dimensions: 10 mm × 7 mm.

(a)

Material	Designation	Type
Cu	L1 (Top)	SIG (Rad. El.)
Isola Astra MT 77	PESA Substrate	
Cu	L2	GND
Prepreg		
Isola Astra MT 77	Feed Substrate	
Cu	L3	SIG (Feed)
Prepreg		
Isola Astra MT 77 (Core)	Feed Substrate	
Cu	L4 (Bottom)	GND

SIGNAL via
GROUND via

(b)

Figure 13. (a) Fabricated antenna and (b) its layer stack structure.

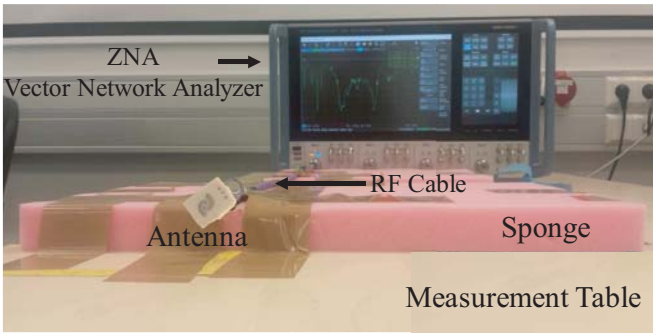

Figure 14. Measurement setup.

Measured data are obtained upon measurements of the reflection coefficient S_{11}. A comparison between simulated and measured data is provided in Fig. 15. Compared to the case without connector, i.e., the case of Fig. 10 with a lumped port at the input, the manufactured antenna shows a reduced impedance bandwidth (18.1 to 25.7 and 29.3 to 32.7 GHz) due to reflections at the junction between the coaxial connector and the stripline. In fact, since the ground plane around the center pin has been cleared, the impedance between the center conductor and the edge of the stripline ground plane has become undefined, resulting in an abrupt flow of the signal current from the center pin to the stripline layer [26]. Moreover, the intersection region between the vertical center conductor and the stripline acts as an antenna, since electric charges moving at uniform velocity along a bent conductor accelerate and radiate.

Experimental and simulated curves do not differ appreciably, which means that measured and simulated values are in good agreement. Discrepancies observed between simulated and experimental

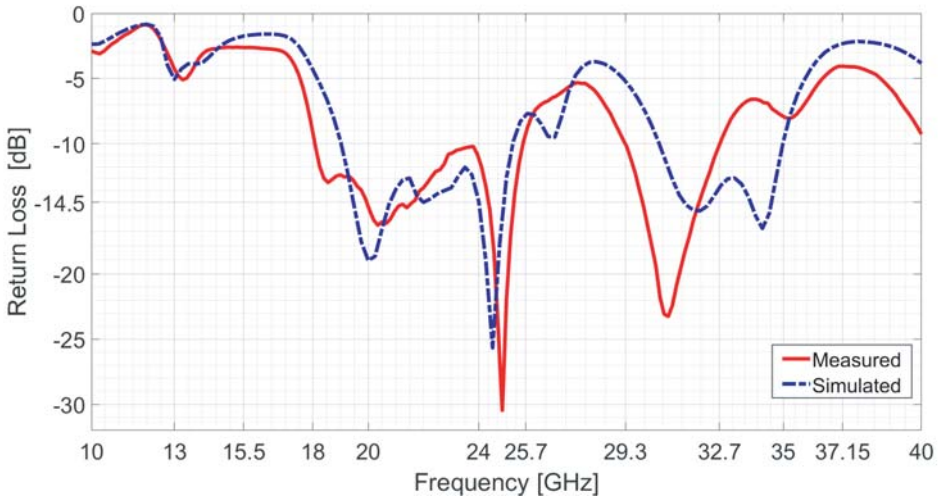

Figure 15. Experimental validation of the approach by comparison of simulated and measured data.

results are due to human-made noise during the manufacturing process and uncertainties during measurement. There is no zero percent error even though all manufacturing process requirements have been taken into account in the simulation.

The authors would have provided additional measured radiation characteristics for comparison. Unfortunately, we do not have an anechoic chamber at our disposal to carry out needed measurements. Nevertheless, given the accuracy and precision of the simulations and the consideration of all factors that can influence the radiation characteristics, there is no doubt that, if carried out, obtained experimental results will corroborate simulated data.

4. CONCLUSION

To avoid pure academic work, when designing antennas for high-frequency applications, manufacturing requirements should be taken into consideration. This requires an application of design methodologies to ease up the process. This work presents a development process that may be used for the implementation of compact planar spiral antennas. General design rules are provided. They encompass selection criteria for dielectric material to be used, aspects to consider when sketching the radiating element design, and those for the implementation of the feeding network. It is shown that the used dielectric material plays a paramount role, as parameters like dielectric loss and substrate thickness influence the overall radiation characteristics of the antenna. A rule of thumb, which may be helpful in the determination of the height of the supporting substrate of the antenna, has been found.

As the feeding network is embedded into the substrate, the mathematical description of the then obtained waveguide and its intrinsic propagation properties were combined to determine the thickness of the waveguide as well as the input and output impedance of the feed and its matching to the radiating element with respect to manufacturing requirements. The rest of the feed was designed using well-known transmission line techniques.

The method presented was applied to a single equiangular spiral antenna element as a case study to demonstrate the approach's validity. A comparison between measured and experimental data shows good agreement. The appeal of the method resides in the fact that it:

- eases up the design process,
- helps minimizing errors and saves time and money since manufacturing requirements are taken into account from the beginning,
- enables the design of compact and small-size spiral antenna as antenna-in-package (AiP), and provides the opportunity to assemble the antenna with other RF components/systems on the same layer stack or on the same integration platform.

Although the method is only applied to two-arm spiral antennas as an example, it is obvious that the method can be extended to four-arm spirals or more, and other antenna geometries.

REFERENCES

1. Chatterjee, J. S., "Radiation Field of a conical helix," *Journal of Applied Physics*, Vol. 24, No. 5, 550–559, May 1953.
2. Turner, E. M., "Spiral slot antenna," U.S. Patent 2,863,145, Dec. 1958.
3. Dyson, J. D., "The non-planar equiangular spiral antenna," *Proc. USAF Antenna Research and Development Program. Symp.*, 1958.
4. Dyson, J. D., "The equiangular spiral antenna," *IRE Trans. Antennas Propag.*, Vol. 7, 181–187, Apr. 1959.
5. Dyson, J. D., "The unidirectional equiangular spiral antenna," *IRE Trans. Antennas Propag.*, Vol. 7, No. 4, 329–334, Oct. 1959.
6. Bawer, R. and J. J. Wolfe, "The spiral antenna," *I.R.E. International Convention Record*, 84–95, Mar. 1960.
7. Curtis, W. L., "Spiral antennas," *IRE Trans. Antennas Propag.*, Vol. 8, No. 3, 298–306, May 1960.
8. Bawer, R. and J. J. Wolfe, "A printed circuit balun for use with spiral antennas," *IRE Trans. on Microwave Theory and Techniques*, Vol. 8, No. 3, 319–325, May 1960.
9. Cheo, B. R. S., V. H. Rumsey, and W. J. Welch, "A solution to the frequency-independent antenna problem," *IRE Trans. Antennas Propag.*, Vol. 7, 527–534, 1961.
10. Deschamps, G. A. and J. D. Dyson, "The logarithmic spiral in a single-aperture multimode antenna system," *IEEE Trans. Antennas Propag.*, Vol. 19, No. 1, 90–96, Jan. 1971.
11. Nakano, H., K. Nogami, S. Arai, H. Mimaki, and J. Yamauchi, "A spiral antenna backed by a conducting plane reflector," *IEEE Trans. Antennas Propag.*, Vol. 34, No. 6, 791–796, Jun. 1986.
12. DuHamel, R. H. and J. P. Scherer, "Frequency independent antennas," *Antenna Engineering Handbook*, 3rd Edition, 14-1–14-68, McGraw-Hill, 1993.
13. Liu, B., "Vertically interconned wide-bandwidth monolithic planar antennas for 3D-IC," Dissertation, University of Cincinnati, 2002.
14. Lee, K. F. and W. Chen, *Advances in Microstrip and Printed Antennas*, John Wiley & Sons, New York, 1997.
15. https:\\www.isola-group.com\wp-content\uploads\data-sheets\Astra_sup_sup_MT77_Dk_Df_-Tables.pdf.
16. http:\\www.contag.de\uploads\pi_ti\technische_ausfuehrung.pdf.
17. Stutzman, W. L. and G. A. Thiele, *Antenna Theory and Design*, 2nd Edition, John Wiley & Sons, New York, 1998.
18. Pozar, D. M., *Microwave Engineering*, 4th Edition, John Wiley & Sons, New York, 2012.
19. Maloratsky, L. G., *Passive RF & Microwave Integrated Circuits*, Elsevier Inc., 2004.
20. Balanis, C. A., *Antenna Theory. Analysis and Design*, 513–514, 3rd Edition, John Wiley & Sons, New York, 2005.
21. Henderson, A. and J. R. James, "Design of microstrip antenna feeds. Part 1: Estimation of radiation loss and design implications," *IEE Proc. H — Microwaves, Optics and Antennas*, Vol. 128, No. 1, Feb. 1981.
22. Hall, P. S. and J. R. James, "Design of microstrip antenna feeds. Part 2: Design and performance limitations of triplate corporate feeds," *IEE Proceedings H — Microwaves, Optics and Antennas*, Vol. 128, No. 1, Feb. 1981.
23. Horng, T. S. and N. G. Alexopoulos, "Corporate feed design for microstrip arrays," *IEEE Trans. Antennas Propag.*, Vol. 41, No. 12, Dec. 1993.
24. Wentworth, S. M. and S. M. Rao, "Analysis of equiangular spiral antennas," *Int. Journal of Microwave and Millimeter-Wave Computer-Aided Engineering*, Vol. 6, No. 2, 92–99, 1996.

25. Sirbu, B., T. Tekin, and D. Pouhè, "Design and simulation of an equiangular spiral antenna for extremely high-frequencies," *Proc. of the 8th European Conference on Antennas and Propagation*, Apr. 6–11, 2014.
26. Holzman, E., *Essentials of RF and Microwave Grounding*, Artech House, Inc., 2006